draft version February 1, 2008, accepted for publication in the Astrophysical Journal
Preprint typeset using LaTeX style emulateapj v. 03/07/07

DETECTION OF EMISSION FROM THE CN RADICAL IN THE CLOVERLEAF QUASAR AT Z=2.56

Dominik A. Riechers[1], Fabian Walter[1], Pierre Cox[2], Christopher L. Carilli[3], Axel Weiss[4], Frank Bertoldi[5], and Roberto Neri[2]

draft version February 1, 2008, accepted for publication in the Astrophysical Journal

ABSTRACT

We report the detection of CN(N=3→2) emission towards the Cloverleaf quasar (z = 2.56) based on observations with the IRAM Plateau de Bure Interferometer. This is the first clear detection of emission from this radical at high redshift. CN emission is a tracer of dense molecular hydrogen gas ($n(\mathrm{H_2}) > 10^4\,\mathrm{cm^{-3}}$) within star–forming molecular clouds, in particular in regions where the clouds are affected by UV radiation. The HCN/CN intensity ratio can be used as a diagnostic for the relative importance of photodissociation regions (PDRs) in a source, and as a sensitive probe of optical depth, the radiation field, and photochemical processes. We derive a lensing–corrected CN(N=3→2) line luminosity of $L'_{\mathrm{CN(3-2)}} = (4.5 \pm 0.5) \times 10^9\,\mathrm{K\ km\,s^{-1}pc^2}$. The ratio between CN luminosity and far–infrared luminosity falls within the scatter of the same relationship found for low–z (ultra–) luminous infrared galaxies. Combining our new results with CO(J=3→2) and HCN(J=1→0) measurements from the literature and assuming thermal excitation for all transitions, we find a CO/CN luminosity ratio of 9.3 ± 1.9 and a HCN/CN luminosity ratio of 0.95 ± 0.15. However, we find that the CN(N=3→2) line is likely only subthermally excited, implying that those ratios may only provide upper limits for the intrinsic 1→0 line luminosity ratios. We conclude that, in combination with other molecular gas tracers like CO, HCN, and HCO^+, CN is an important probe of the physical conditions and chemical composition of dense molecular environments at high redshift.

Subject headings: galaxies: active, starburst, formation, high redshift — cosmology: observations — radio lines: galaxies

1. INTRODUCTION

Investigations of the dense molecular interstellar medium (ISM) in high–redshift galaxies are of fundamental importance to further our understanding of the early phases of galaxy formation and evolution, as it harbors the environments in which the actual star formation is believed to occur. Recent studies of the molecular gas phase in high–z galaxies using CO emission lines have revealed large molecular gas reservoirs with masses in excess of $10^{10}\,\mathrm{M_\odot}$ (see review by Solomon & Vanden Bout 2005, and references therein).

However, while the relative brightness of CO emission lines renders this molecule the most common tracer of the requisite material for star formation, the low densities of only $n_{\mathrm{H_2}} \sim 10^2 - 10^3\,\mathrm{cm^{-3}}$ required to excite its lower–J transitions (due to its low dipole moment of only $\mu_{\mathrm{D}}^{\mathrm{CO}} = 0.11$) imply that CO is not a specific tracer of dense molecular cloud cores, i.e., the regions where stars are actively formed.

In contrast, recent studies of nearby actively star–forming galaxies have shown that the high dipole molecule HCN ($\mu_{\mathrm{D}}^{\mathrm{HCN}} = 2.98$) is a far better tracer of such dense molecular cores (e.g. Gao & Solomon 2004a, 2004b). The critical density of $n_{\mathrm{H_2}} \sim 10^5 - 10^6\,\mathrm{cm^{-3}}$ to collisionally thermalize its lower–J transitions is much higher than that of CO, and of the same order as the densities found in bright star–forming regions in the Galaxy (e.g. the Orion Bar, Hogerheijde et al. 1995). A main result in this context is the finding that the HCN luminosity correlates well with the far–infrared (FIR) luminosities (which is commonly used to estimate star–formation rates at high redshift) over 7–8 orders of magnitude, from Galactic dense cores to the highest redshift quasars (Wu et al. 2005).

However, in nearby luminous and ultra–luminous infrared galaxies (LIRGs/ULIRGs), it has been found that systems with similar HCN/CO and HCN/FIR luminosity ratios may have quite different dense gas properties regarding their chemical composition, and their gas excitation (e.g., Aalto et al. 2002). To better understand the physical and chemical state of the dense molecular gas phase which directly relates to star formation, it has proven essential to study additional bright tracers of dense gas with properties different from HCN, such as the cyanide radical (CN). Due to its lower dipole moment relative to HCN ($\mu_{\mathrm{D}}^{\mathrm{CN}} = 1.45$), its critical density is lower by about a factor of 5. Observations of CN emission toward the Orion A molecular cloud complex have shown that CN filaments trace the dense interfaces between the molecular cloud and the major ionization fronts (Rodríguez–Franco et al. 1998). It has also been found that the [CN]/[HCN] abundance ratio is greatly enhanced in the central region of the starburst galaxy M82, being as high as ∼5 across the entire nucleus (Fuente et al. 2005). These observations indicate that CN is a good tracer of gas layers which are

Electronic address: riechers@mpia.de
[1] Max-Planck-Institut für Astronomie, Königstuhl 17, Heidelberg, D-69117, Germany
[2] Institut de RadioAstronomie Millimétrique, 300 Rue de la Piscine, Domaine Universitaire, 38406 Saint Martin d'Héres, France
[3] National Radio Astronomy Observatory, PO Box O, Socorro, NM 87801, USA
[4] Max-Planck-Institut für Radioastronomie, Auf dem Hügel 69, Bonn, D-53121, Germany
[5] Argelander-Institut für Astronomie, Universität Bonn, Auf dem Hügel 71, Bonn, D-53121, Germany

affected by photochemistry, since this molecule appears to be predominantly found in regions exposed to ionizing stellar UV radiation. It has also been found that, due to the rapid destruction of other dense gas tracers like HCN, the abundance of CN tends to be enhanced in areas where the UV radiation field is only partly attenuated, such as in zones close to the surface of photodissociation regions (PDRs, Fuente et al. 1993; Sternberg & Dalgarno 1995; Jansen et al. 1995). The CN/HCN intensity ratio can thus be used as a diagnostic for the relative importance of PDRs in a source, and a sensitive probe of optical depth, the radiation field, and photochemical processes (e.g., Boger & Sternberg 2005). CN emission may thus in a sense be a more specific tracer for star formation than, e.g., HCN, which only traces regions of dense gas in general. In addition, theoretical studies of the chemical composition of molecular gas for different ionization parameters suggest that the relative abundance of CN may also be enhanced in X–ray dominated regions (XDRs), such as AGN environments (Lepp & Dalgarno 1996). This exemplifies why it is desirable to search for CN emission, which is part of our current effort to study molecular tracers other than CO out to high redshifts. Such an investigation is imperative to obtain more meaningful constraints on the physical properties and chemical composition of the dense molecular ISM in distant galaxies.

In this paper, we report the first high–z detection of CN(N=3→2) emission, which was observed towards the Cloverleaf quasar ($z = 2.56$) with the IRAM Plateau de Bure Interferometer (PdBI)[6]. Due to its strong gravitational magnification (magnification factor $\mu_{\rm L} = 11$, Venturini & Solomon 2003), the Cloverleaf is the brightest CO source at high redshift (e.g., Barvainis et al. 1994), and one of the most prolific sources of molecular lines beyond z=2. It was the first $z > 2$ source to be detected in HCN (Solomon et al. 2003) and HCO^+ (Riechers et al. 2006a) emission. It was also detected in both C I fine structure lines (Barvainis et al. 1997; Weiß et al. 2003, 2005). We use a standard concordance cosmology throughout, with $H_0 = 71$ km s^{-1} Mpc^{-1}, $\Omega_{\rm M} = 0.27$, and $\Omega_\Lambda = 0.73$ (Spergel et al. 2003, 2007).

2. OBSERVATIONS

We observed the CN(N=3→2) transition line ($\nu_{\rm rest}$ = 339.4467770 − 340.2791661 GHz for the different fine structure [fs] and hyperfine structure [hfs] transitions of the v=0 vibrational state) towards H1413+117 (the Cloverleaf quasar) using the PdBI in D configuration between 2006 July 26 and September 03. At the target redshift of z=2.55784 (Weiß et al. 2003), the line is shifted to ∼95.6 GHz (3.14 mm). The total integration time amounts to 17.5 hr using 5 antennas, resulting in 5.8 hr equivalent on–source time with 6 antennas after discarding unusable visibility data. The nearby sources 1354+195 and 1502+106 (distance to the Cloverleaf: 9.0° and 12.0°) were observed every 20 minutes for pointing, secondary amplitude and phase calibrations. For primary flux calibration, several nearby calibrators (MWC 349, CRL 618, 3C 273, 3C 345, and NRAO 150) were observed during all runs.

[6] IRAM is supported by INSU/CNRS (France), MPG (Germany), and IGN (Spain).

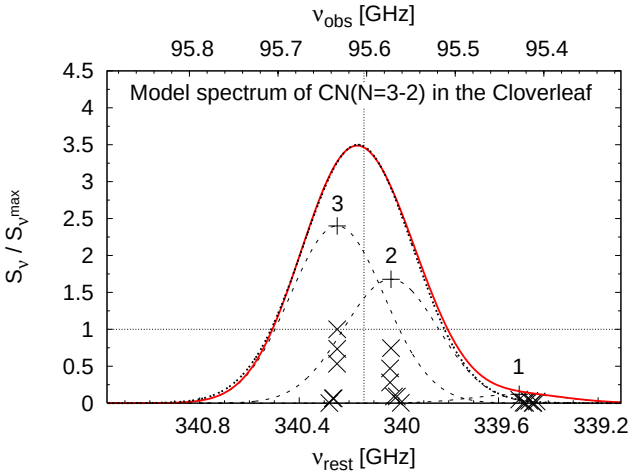

FIG. 1.— Model spectrum of the CN(N=3→2) emission in the Cloverleaf. The horizontal axes indicate the rest and observed frequencies. The full range of the PdBI bandpass is shown. The vertical axis indicates the predicted intensity, normalized to the (N=3→2, J=$\frac{7}{2}$→$\frac{5}{2}$, F=$\frac{9}{2}$→$\frac{7}{2}$) component. The relative intensities are computed for the LTE case. The crosses indicate the hyperfine structure components. The plus signs indicate the summed intensities of the components in three different frequency bins. The dashed lines are Gaussian fits to the summed intensities, assuming the width of the CO(J=3→2) line (Weiß et al. 2003) for the subcomponents (labeled '1'–'3'). The solid line is a sum of all three components, and indicates the model–predicted CN(N=3→2) line shape. The thick dotted line is a single Gaussian (used to fit the observations), fitted to the model line. The dotted vertical line indicates the tuning frequency, corresponding to zero velocity in Fig. 4.

The correlator was tuned to a frequency of 95.603 GHz, which corresponds to the central position between the brightest hfs transitions[7] of the CN(N=3→2) line at 95.6332 and 95.5736 GHz. The total bandwidth of 580 MHz (∼1800 km s^{-1}) used for the observations is large enough to cover all fs and hfs transitions of the CN(N=3→2) line. It also covers enough channels that are free of line emission to constrain the 3 mm continuum emission of the Cloverleaf.

For data reduction and analysis, the IRAM GILDAS package was used. All data were mapped using the CLEAN algorithm and 'natural' weighting without applying a further taper; this results in a synthesized beam of 5.3″×4.9″ (∼42 kpc at $z = 2.56$). The final rms in the combined map is 0.25 mJy beam^{-1} for a 190 MHz (corresponding to 596 km s^{-1}) channel, 0.4 mJy beam^{-1} for a 80 MHz (252 km s^{-1}) channel, and 0.8 mJy beam^{-1} for a 20 MHz (63 km s^{-1}) channel.

3. THEORETICAL CONSIDERATIONS

Due to its fine stucture and hyperfine structure splitting, the CN(N=3→2) emission line is distributed over 19 lines[8], in 3 main components separated by more than

[7] These components are actually blends of the [N=3→2, J=$\frac{5}{2}$→$\frac{3}{2}$, (F=$\frac{7}{2}$→$\frac{5}{2}$, $\frac{5}{2}$→$\frac{3}{2}$, and $\frac{3}{2}$→$\frac{1}{2}$)] hfs components at $\nu_{\rm rest}$ = 340.0315440 − 340.0354080 GHz and [N=3→2, J=$\frac{7}{2}$→$\frac{5}{2}$, (F=$\frac{9}{2}$→$\frac{7}{2}$, $\frac{7}{2}$→$\frac{5}{2}$, and $\frac{5}{2}$→$\frac{3}{2}$)] hfs components at $\nu_{\rm rest}$ = 340.2477700 − 340.2485764 GHz (components 2 and 3 in Fig. 1).

[8] We assume that CN is in its ground electronic state ($^2\Sigma$), and that the spins couple according to Hund's case (b) coupling scheme: $\vec{N}+\vec{S}=\vec{J}$, (fs coupling) and $\vec{J}+\vec{I_{\rm C}}+\vec{I_{\rm N}}=\vec{F}$ (hfs coupling). Here, $\vec{N}$ is the rotational angular momentum vector, $\vec{S}$ is the electronic spin, and $\vec{I}$ is a nuclear spin.

200 MHz from each other in the rest frame. This separation is of the same order as the kinematical broadening of the CO lines in the Cloverleaf (Weiß et al. 2003), causing the hfs components to be blended. To analyze the intrinsic line shape of the CN(N=3→2) transition in the Cloverleaf, we calculated a synthetic line profile, assuming optically thin emission in Local Thermodynamic Equilibrium (LTE) to derive the relative intensities of the hfs components. The relative intensities of the components were computed using the laboratory data from Skatrud et al. (1983), and approximation (4) of equation (1) of Pickett et al. (1998). Assuming that the 3 main CN(N=3→2) components are kinematically broadened in the same way as the CO lines (416 ± 6 km s^{-1} FWHM; see Weiß et al. 2003), we obtain the synthetic line profile displayed in Fig. 1 (solid line). Under the given assumptions, the contribution from all hfs lines of component 1 to the total intensity are negligible, and not detectable at the given signal–to–noise (see below). A single Gaussian fit (dotted line, 484 km s^{-1} FWHM, or 116% of the CO lines) agrees with the more detailed model profile (solid line) within a few percent in its peak position and integral, i.e., well within the observational errors. Note however that the width and peak position of this Gaussian depends on the relative intensities of the hfs components, which in turn depend on the above assumptions, in particular the optical depth. In the optically thin LTE case, components 2 and 3 have a peak strength ratio of 1:1.4. As an example, if they had a ratio of unity, the fitted Gaussian to the line profile would have a FWHM of 603 km s^{-1}, or 145% of the CO lines. We thus conclude that fitting a Gaussian to the observed line profile contains all relevant information, while minimizing the number of free fit parameters, and thus is preferred over a more complex fitting procedure to describe and analyze the CN(N=3→2) profile at the given signal–to–noise ratio.

4. RESULTS

4.1. *CN Maps and Spectrum*

We have detected emission from the CN(N=3→2) transition line towards the Cloverleaf quasar (z = 2.56). The velocity–integrated CN(N=3→2) line map is shown in Fig. 2. The cross indicates the geometrical center position of the resolved CO(J=7→6) map at α = 14$^{\rm h}$15$^{\rm m}$46$^{\rm s}$.233, δ = +11°29′43″.50 (Alloin et al. 1997). The line emission is clearly detected at 7σ over a range of 596 km s^{-1} (190 MHz); the source appears unresolved. In Fig. 3, six channel maps (252 km s^{-1}, or 80 MHz each) of the CN(N=3→2) line emission are shown. At an rms of 0.4 mJy beam^{-1}, the line is detected at 4 and 5σ in the central channels, and the decline of the line intensity towards the line wings is clearly visible toward the outer channels, as expected.

Fig. 4 shows the spectrum of the CN(N=3→2) emission at a resolution of 63 km s^{-1} (20 MHz). Zero velocity corresponds to the tuning frequency of 95.603 GHz. The solid line shows a Gaussian fit to the spectrum. From the fit, we derive a line peak flux density of 1.94 ± 0.24 mJy beam^{-1}, and a line FWHM of 666 ± 97 km s^{-1}. The fit provides an upper limit for the continuum emission at the line frequency of <0.25 mJy. From the channels assumed to be free of line emission, we derive a formal 3σ upper limit to the continuum peak flux density of 0.7 mJy beam^{-1}. Note that the model fit to the dust SED of the Cloverleaf by Weiß et al. (2003) would suggest a continuum flux of ∼0.3 mJy at the CN(N=3→2) line frequency, which agrees within the errors with the above estimates. As the continuum however is not detected, we do not subtract a continuum component from the observed spectrum. This leads to an integrated CN(N=3→2) line flux of 1.37 ± 0.17 Jy km s^{-1}. The velocity offset of the Gaussian peak relative to the tuning frequency is -105 ± 38 km s^{-1}.

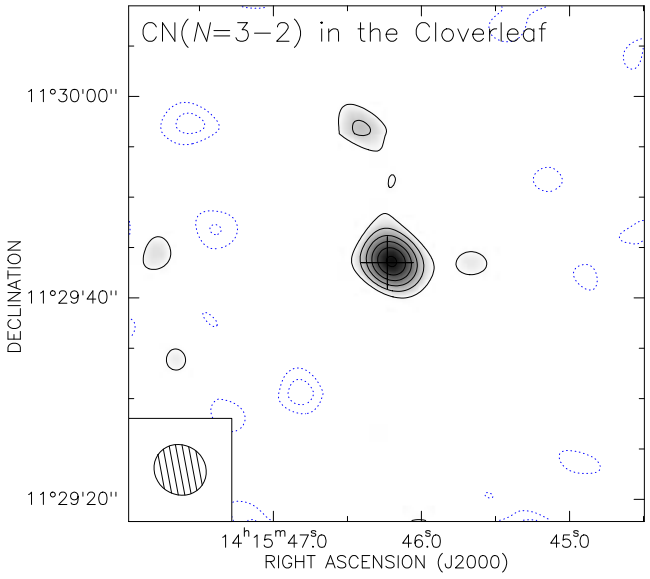

FIG. 2.— Velocity–integrated PdBI map of CN(N=3→2) emission towards the Cloverleaf quasar. At a resolution of 5.3″×4.9″ (as indicated in the bottom left corner), the source is unresolved. The cross indicates the geometrical center of the CO emission in the Cloverleaf (Alloin et al. 1997, see text). Contours are shown at (-3, -2, 2, 3, 4, 5, 6, 7)×σ (1σ = 0.25 mJy beam^{-1}).

The FWHM of the Gaussian fit to the CN(N=3→2) emission line suggests that its components 2 and 3 have similar peak strengths (different from 1:1.4 as predicted for the optically thin LTE case; Fig. 1), which may indicate that the emission is optically thick. Within the limited signal–to–noise of the spectrum, the shape of the emission line remains compatible with a two–component structure. It may thus be possible that the two brightest hfs complexes (components 2 and 3) are detected individually, but observations at higher signal–to–noise are needed to confirm this result. In any case, a double Gaussian fit to the line profile gives the same integrated line flux as the single Gaussian fit within the errors.

4.2. *Line Luminosities*

From our observations, we derive a CN(N=3→2) line luminosity of $L'_{\rm CN(3-2)} = (4.5 \pm 0.5) \times 10^9$ K km s^{-1} pc^2 (corrected for gravitational magnification, $\mu_{\rm L}$ = 11; see Table 1 for details). This corresponds to 11% of $L'_{\rm CO(3-2)}$ (Weiß et al. 2003), 105% of $L'_{\rm HCN(1-0)}$ (Solomon et al. 2003), and 129% of $L'_{\rm HCO^+(1-0)}$ (Riechers et al. 2006a). Assuming that CN is thermally excited up to the N=3→2 transition (i.e., $L'_{\rm CN(3-2)} = L'_{\rm CN(1-0)}$) and that optical depth effects can be neglected, this would mean that CN emission in the Cloverleaf is slightly brighter than that from the other high density probes HCN and

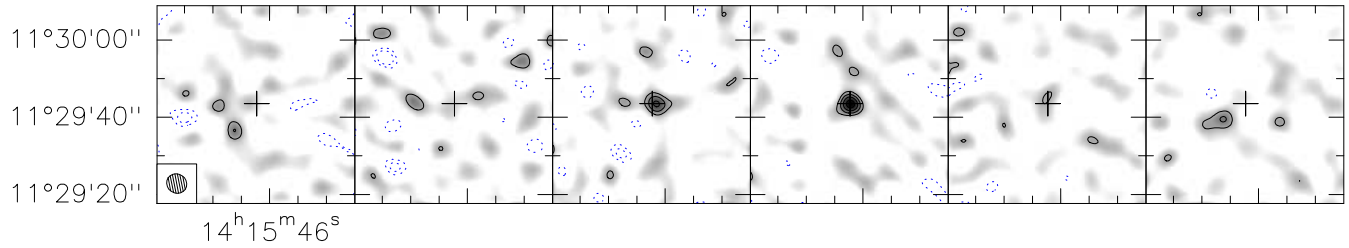

FIG. 3.— Channel maps of the CN(N=3→2) emission (same region is shown as in Fig. 2). One channel width is 80 MHz, or 252 km s^{-1} (at 95.4355, 95.5155, 95.5955, 95.6755, 95.7555, and 95.8355 GHz; frequencies increase with channel number). Contours are shown at (-3, -2, 2, 3, 4, 5)×σ (1σ = 0.4 mJy beam^{-1}). The beam size (5.3″×4.9″) is shown in the bottom left corner; the cross indicates the same position as in Fig. 2.

HCO$^+$. This is remarkable, as HCN and HCO$^+$ have higher critical densities than CN in the ground–state transition, but the critical density of CN(N=3→2) is higher than that of HCN(J=1→0) and HCO$^+$(J=1→0). This may indicate a higher relative filling factor of CN relative to HCN and HCO$^+$, or even a relatively high chemical abundance of CN. However, with the observations existing at present, it is not possible to disentangle excitation effects from chemical effects.

In addition, observations of HCN(J=4→3) towards the Cloverleaf quasar have shown that $L'_{\rm HCN(4-3)}/L'_{\rm HCN(1-0)} \leq 0.34$ (Solomon et al. 2003, caption of their Tab. 1, and M. Guélin 2007, priv. comm.). This ratio is significantly lower than 1, which implies that the 4→3 transition of HCN is sub–thermally excited. As the CN(N=3→2) transition has a somewhat lower but comparable critical density relative to HCN(J=4→3), it is likely that the CN(N=3→2) transition is also sub–thermally excited, and the 'intrinsic', thermalization–corrected $L'_{\rm CN(1-0)}$ thus even higher. This would be consistent the finding that CN is clearly subthermally excited in nearby LIRGs and ULIRGs (Aalto et al. 2002). This would also imply that CN is a *brighter* tracer of dense gas than HCN and HCO$^+$ in this high redshift quasar.

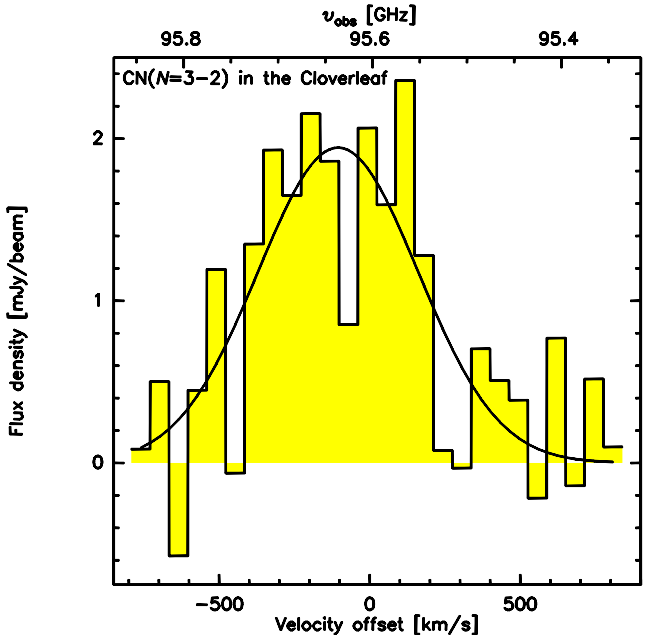

FIG. 4.— Spectrum of the CN(N=3→2) emission at a resolution of 63 km s^{-1} (20 MHz). The velocity scale is relative to the tuning frequency of 95.603 GHz. The rms per velocity bin is 0.8 mJy. The solid line shows a Gaussian fit to the data.

TABLE 1
MOLECULAR LINE LUMINOSITIES IN THE CLOVERLEAF.

	S_ν [mJy]	L' [10^9 K km s^{-1} pc^2]	Ref.
CN(N=3→2)	1.94 ± 0.24	4.5 ± 0.5	1
HCN(J=1→0)	0.24 ± 0.04	4.3 ± 0.5	2
HCO$^+$(J=1→0)	0.19 ± 0.03	3.5 ± 0.3	3
CO(J=3→2)	30 ± 1.7	42 ± 7	4

REFERENCES. — [1] This work, [2] Solomon et al. (2003), [3] Riechers et al. (2006a), [4] Weiß et al. (2003).
NOTE. — Luminosities are corrected for gravitational magnification.

5. DISCUSSION

In the following, we discuss various relationships between the emission observed in CN and other molecules (CO and HCN) and the far–IR continuum for a sample of local spiral/starburst galaxies (Henkel et al. 1988, 1998, 2007, priv. comm.; Wang et al. 2004; additional CO/HCN/FIR data from Eckart et al. 1990; Nguyen-Q-Rieu et al. 1992; Mauersberger et al. 1996; Mao et al. 2000; Sanders et al. 2003), low–z (U)LIRGs (Aalto et al. 2002), and the Cloverleaf (this work; Solomon et al. 2003; Weiß et al. 2003) as shown in Fig. 5. Note that, due to the weak signal–to–noise ratio of 1σ, we do not include the CN(N=4→3) observations of APM 08279+5255 (Guelin et al. 2007, their Tab. 1) in this discussion.

As CO(J=1→0) is not yet detected toward the Cloverleaf, we assume in the following that CO is thermalized up to the 3→2 transition, i.e., $L'_{\rm CO(1-0)} = L'_{\rm CO(3-2)}$ (see Riechers et al. 2006b for justification). Both effects of thermal and sub–thermal excitation of the CN(N=3→2) emission line in the Cloverleaf are discussed. CO, CN, and HCN line intensities for all low–z galaxies were measured directly in the ground–state transitions, all quoted luminosities thus are 1→0 luminosities. We do not discuss effects of differential lensing[9], as models indicate similar sizes for molecular and dust emission in the Cloverleaf (Solomon et al. 2003).

Figure 5a: Wu et al. (2005) find a linear correlation between $L'_{\rm HCN}$ and $L_{\rm FIR}$ over 7–8 orders of magnitude in luminosity, which is believed to indicate that the dense gas tracer HCN is also a good estimator for star formation rates out to high z. If CN were to be a good tracer

[9] Note that Chartas et al. (2007) recently reported a likely microlensing event toward the Cloverleaf; however, this event took place close to 2000 April, so 3–7 years before all of the molecular gas observations of this source discussed in this paper (obtained between 2003 March and 2006 September).

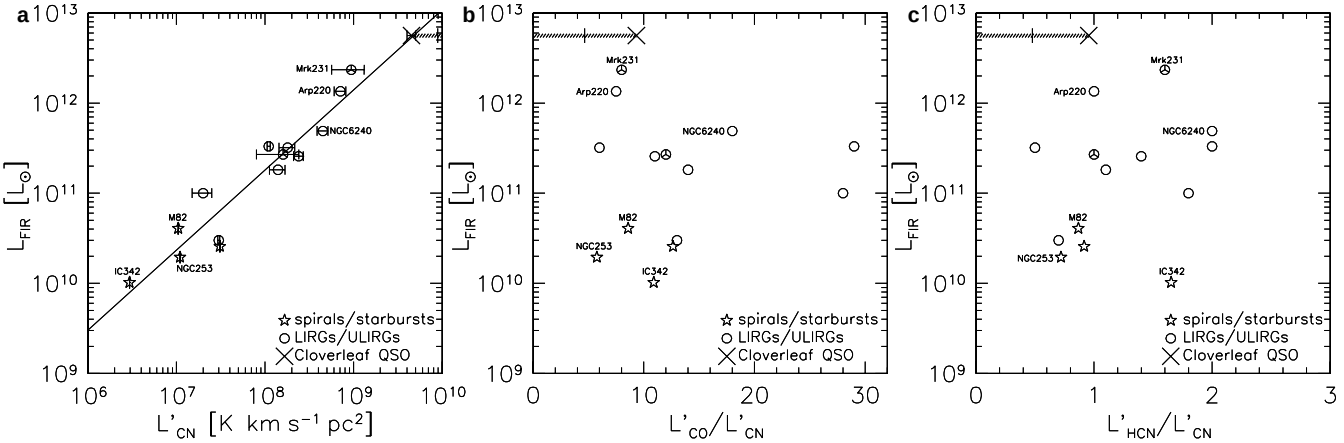

FIG. 5.— CN luminosity relations for a sample of local spiral/starburst galaxies, low–z IR–luminous galaxies, and the Cloverleaf. The Cloverleaf luminosities are corrected for gravitational lensing ($\mu_L = 11$). The two symbols with star insets denote tentative CN detections. The solid line is a least squares fit to all data except the Cloverleaf. The error bars indicate the statistical errors of the line luminosity measurements. The excitation of the CN(N=3→2) transition in the Cloverleaf may be sub–thermal, which would affect the (extrapolated) CN(N=1→0) line luminosity as indicated by the horizontal, shaded regions. As an example, the vertical bars on the shaded regions show a case where $L'_{\rm CN(3-2)} = 0.5 \times L'_{\rm CN(1-0)}$ in the Cloverleaf. See text for more details.

of dense, actively star–forming gas, a similar trend may be expected between $L'_{\rm CN}$ and $L_{\rm FIR}$. Figure 5a shows that $L'_{\rm CN}$ correlates closely with $L_{\rm FIR}$; a linear least squares fit to all galaxies (excluding the Cloverleaf) yields $\log(L_{\rm FIR}) = (0.89 \pm 0.09) \times \log(L'_{\rm CN}) + (4.2 \pm 0.7)$. This slope may suggest a trend of decreasing CN/FIR luminosity ratio towards higher luminosities (see also Aalto et al. 2002). It however also is consistent with unity within the statistical uncertainties (which are quite large due to the limited sample size) and systematical errors (e.g., different beam sizes for CN line and IR continuum observations), and thus with CN being a valuable tracer of star formation. The Cloverleaf agrees remarkably well with the relation defined by the low–z galaxies (even if the CN(N=3→2) transition is sub–thermally excited, as indicated by the horizontal bar on the shaded region), extending the observed trend to higher luminosities and out to high redshift.

Figure 5b: Gao & Solomon (2004b) observe a rise in dense gas fraction with $L_{\rm FIR}$. The $L'_{\rm CO}/L'_{\rm CN}$ ratio may be considered (the inverse of) a tracer of the dense gas fraction. A significant spread in the $L'_{\rm CO}/L'_{\rm CN}$ ratio is found for the sample shown in Fig. 5b, ranging from a few to almost a factor of 30. There is no obvious trend of $L'_{\rm CO}/L'_{\rm CN}$ with $L_{\rm FIR}$; however, the sample size is too small and heterogenous to come to a definite conclusion. Note that, due to the likely sub–thermal excitation of the CN(N=3→2) transition (as indicated by the shaded region), the $L'_{\rm CO}/L'_{\rm CN}$ ratio may be considered an upper limit of the 'intrinsic', thermalization–corrected ratio of the 1→0 transitions for the Cloverleaf.

Figure 5c: Assuming that CN traces the UV field (which falls off rapidly with growing distance from star–forming regions, or an active galactic nucleus), while HCN traces dense gas in general, it would be expected that the HCN/CN ratio stays constant or decreases with increasing $L_{\rm FIR}$. In this scenario, a decrease in the HCN/CN ratio would correspond to an increase in the filling factor of UV–illuminated clouds with $L_{\rm FIR}$. This would however also cause a rise in $L'_{\rm CN}/L_{\rm FIR}$, which is not observed (Fig. 5a). If differences in the relative chemical abundances of CN and HCN and optical depth/thermalization effects do not play a major role, one may thus expect $L'_{\rm HCN}/L'_{\rm CN}$ to stay fairly constant with $L_{\rm FIR}$. Based on the observations of their subsample, Aalto et al. (2002) suggest that the HCN/CN intensity ratio may increase slightly with $L_{\rm FIR}$. Such a trend however is not seen in the larger sample displayed in Fig. 5c (note that $L'_{\rm HCN}/L'_{\rm CN}$ for the Cloverleaf may again be considered an upper limit due to possible sub–thermal excitation of CN(N=3→2), as indicated by the shaded region). Clearly, improved statistics and better models are required to address this issue in more detail.

Chemical models suggest that CN is produced quite efficiently in the presence of a strong UV field, which also leads to an enhanced ionization rate (Boger & Sternberg 2005). The large observed [CN]/[HCN] abundance ratio of ∼5 toward the molecular disk of M82 may be indicative of a large dense PDR bathed in the intense radiation field of the starburst environment (Fuente et al. 2005), lending observational support to these models. Other models suggest that the relative abundance of CN may also be enhanced in regions with elevated X–ray ionization rates, such as AGN environments (Lepp & Dalgarno 1996; Meijerink & Spaans 2005). Especially in the Cloverleaf, where the central quasar is known to contribute a significant fraction to the heating of the gas and dust (Weiß et al. 2003; Solomon et al. 2003), such a scenario would appear reasonable and may explain the relatively high brightness of CN compared to other dense gas tracers in the Cloverleaf. However, note that in Fig. 5c, the pure starburst galaxies show the brightest CN emission relative to HCN, and galaxies with a relatively strong AGN like Mrk 231 and NGC 6240 have some of the highest $L'_{\rm HCN}/L'_{\rm CN}$ ratios. This may indicate that the strength of the UV field in a starburst environment has a significantly greater impact on the global gas–phase production rate of CN in a galaxy than the strength of the X–ray field, lending further support to the supposition that CN is a good star formation tracer. We thus conclude that the XDR scenario alone does not explain the observed dense gas properties of the (U)LIRGs shown in Fig. 5 without any further assumptions.

Overall, the Cloverleaf follows the $L'_{\rm CN}$–$L_{\rm FIR}$ relation

as defined by nearby galaxies of different types remarkably well, and extends this relation to higher luminosities. This relation now appears to hold over almost 3 orders of magnitude. If these findings were to hold for other distant quasars, CN would be an excellent probe of dense molecular environments out to high redshifts. Also, the higher–order transitions of CN appear to be brighter than those of other dense gas tracers like HCN. This may prove to be of particular importance for future high–z studies with the Atacama Large Millimeter/submillimeter Array (ALMA), which will offer the opportunity to probe to fainter galaxy populations in general, but will also be restricted to the higher–order transitions of the most common dense molecular gas tracers (typically 3→2 and higher at $z > 2$).

This research is based on observations carried out with the IRAM Plateau de Bure Interferometer. IRAM is supported by INSU/CNRS (France), MPG (Germany), and IGN (Spain). D. R. acknowledges support from the Deutsche Forschungsgemeinschaft (DFG) Priority Programme 1177. C. C. acknowledges support from the Max-Planck-Gesellschaft and the Alexander von Humboldt-Stiftung through the Max-Planck-Forschungspreis 2005. The authors would like to thank Susanne Aalto for fruitful discussions on the subject matter. We also would like to thank the staff at IRAM, in particular Jan Martin Winters, for their assistance in setting up and carrying out the observations, as well as for providing a preliminary reduction of the data. The authors would like to thank the referee for useful comments that helped to improve the manuscript.

REFERENCES

Aalto, S., Polatidis, A. G., Hüttemeister, S., & Curran, S. J. 2002, A&A, 381, 783
Alloin, D., Guilloteau, S., Barvainis, R., Antonucci, R., & Tacconi, L., 1997, A&A, 321, 24
Barvainis, R., Tacconi, L., Antonucci, R., Alloin, D., & Coleman, P. 1994, Nature, 371, 586
Barvainis, R., Maloney, P., Antonucci, R., & Alloin, D. 1997, ApJ, 484, 695
Boger, G. I., & Sternberg, A. 2005, ApJ, 632, 302
Chartas, G., Eracleous, M., Dai, X., Agol, E., & Gallagher, S. 2007, ApJ, in press (astro-ph/0702742)
Eckart, A., Downes, D., Genzel, R., Harris, A. I., Jaffe, D. T., & Wild, W. 1990, ApJ, 348, 434
Fuente, A., Martin-Pintado, J., Cernicharo, J., & Bachiller, R. 1993, A&A, 276, 473
Fuente, A., García-Burillo, S., Gerin, M., Teyssier, D., Usero, A., Rizzo, J. R., & de Vicente, P. 2005, ApJ, 619, L155
Gao, Y., & Solomon, P. M. 2004a, ApJS, 152, 63
Gao, Y., & Solomon, P. M. 2004b, ApJ, 606, 271
Guélin, M., Salomé, P., Neri, R., García-Burillo, S., Graciá-Carpio, J., et al. 2007, A&A, 462, L45
Henkel, C., Schilke, P., & Mauersberger, R. 1988, A&A, 201, L23
Henkel, C., Chin, Y.-N., Mauersberger, R., & Whiteoak, J. B. 1998, A&A, 329, 443
Hogerheijde, M. R., Jansen, D. J., & van Dishoeck, E. F. 1995, A&A, 294, 792
Jansen, D. J., van Dishoeck, E. F., Black, J. H., Spaans, M., & Sosin, C. 1995, A&A, 302, 223
Lepp, S., & Dalgarno, A. 1996, A&A, 306, L21
Mao, R. Q., Henkel, C., Schulz, A., Zielinsky, M., Mauersberger, R., Störzer, H., Wilson, T. L., Gensheimer, P. 2000, A&A, 358, 433
Mauersberger, R., Henkel, C., Wielebinski, R., Wiklind, T., & Reuter, H.-P. 1996, A&A, 305, 421
Meijerink, R., & Spaans, M. 2005, A&A, 436, 397
Nguyen-Q-Rieu, Jackson, J. M., Henkel, C., Truong-Bach, & Mauersberger, R. 1992, ApJ, 399, 521
Pickett, H. M., Poynter, R. L., Cohen, E. A., Delitsky, M. L., Pearson, J. C., & Müller, H. S. P. 1998, J. Quant. Spectrosc. Radiat. Transfer, 60, 883
Riechers, D. A., Walter, F., Carilli, C. L., Weiß A., Bertoldi, F., Menten, K. M., Knudsen, K. K., & Cox, P. 2006a, ApJ, 645, L13
Riechers, D. A., Walter, F., Carilli, C. L., et al. 2006b, ApJ, 650, 604
Rodriguez-Franco, A., Martin-Pintado, J., & Fuente, A. 1998, A&A, 329, 1097
Sanders, D. B., Mazzarella, J. M., Kim, D.-C., Surace, J. A., & Soifer, B. T. 2003, AJ, 126, 1607
Skatrud, D. D., de Lucia, F. C., Blake, G. A., & Sastry, K. V. L. N. 1983, J. Mol. Spectrosc., 99, 35
Solomon, P., Vanden Bout, P., Carilli, C., & Guelin, M. 2003, Nature 426, 636
Solomon, P. M., & Vanden Bout, P. A. 2005, ARA&A, 43, 677
Spergel, D. N., Verde, L., Peiris, H. V., et al. 2003, ApJS, 148, 175
Spergel, D. N., Bean, R., Doré, O., et al. 2007, ApJ, in press (astro-ph/0603449)
Sternberg, A., & Dalgarno, A. 1995, ApJS, 99, 565
Venturini, S., & Solomon, P. M. 2003, ApJ, 590, 740
Wang, M., Henkel, C., Chin, Y.-N., et al. 2004, A&A, 422, 883
Weiß, A., Henkel, C., Downes, D., & Walter, F. 2003, A&A, 409, L41
Weiß, A., Downes, D., Henkel, C., & Walter, F. 2005, A&A, 429, L25
Wu, J., Evans II, N. J., Gao, Y., Solomon, P. M., Shirley, Y. L., & Vanden Bout, P. A. 2005, ApJ, 635, L173